Theory of the Earth

Don L. Anderson

Chapter 7. Nonelastic and Transport Properties

Boston: Blackwell Scientific Publications, c1989

Recommended citation:

Anderson, Don L. Theory of the Earth. Boston: Blackwell Scientific Publications, 1989. http://resolver.caltech.edu/CaltechBOOK:1989.001

A scanned image of the entire book may be found at the following persistent URL:

http://resolver.caltech.edu/CaltechBook:1989.001

Abstract:

Most of the Earth is solid, and much of it is at temperatures and pressures that are difficult to achieve in the laboratory. The Earth deforms anelastically at small stresses and, over geological time, this results in large deformations. Most laboratory measurements are made at high stresses, high strain rates and low total strain. Laboratory data must therefore be extrapolated in order to be compared with geophysical data, and this requires an understanding of solid-state physics. In this chapter I discuss transport and activated processes in solids, processes that are related to rates or time. Some of these are more dependent on temperature than those treated in previous chapters. These properties give to geology the "arrow of time" and an irreversible nature.

7

Nonelastic and Transport Properties

Shall not every rock be removed out of his place?

—JOB 18:4

Most of the Earth is solid, and much of it is at temperatures and pressures that are difficult to achieve in the laboratory. The Earth deforms anelastically at small stresses and, over geological time, this results in large deformations. Most laboratory measurements are made at high stresses, high strain rates and low total strain. Laboratory data must therefore be extrapolated in order to be compared with geophysical data, and this requires an understanding of solid-state physics. In this chapter I discuss transport and activated processes in solids, processes that are related to rates or time. Some of these are more dependent on temperature than those treated in previous chapters. These properties give to geology the "arrow of time" and an irreversible nature.

THERMAL CONDUCTIVITY

There are three mechanisms contributing to thermal conductivity $\mathcal{K}$ in the crust and mantle. The lattice part, $\mathcal{K}_L$, is produced by diffusion of thermal vibrations in a crystalline lattice and is also called the phonon contribution. $\mathcal{K}_R$ is the radiative part, due to the transfer of heat by infrared electromagnetic waves. If the mantle is sufficiently transparent, $\mathcal{K}_R$ is significant. $\mathcal{K}_E$ is the exciton part, due to the transport of energy by quasiparticles composed of electrons and positive holes. This becomes dominant in intrinsic semiconductors as the temperature is raised. Thus, thermal conduction in solids arises partly from electronic and partly from atomic motion and, at high temperature, from radiation passing through the solid.

Introduction

Debye regarded a solid as a system of coupled oscillators transmitting thermoelastic waves. For an ideal lattice with simple harmonic motion of the atoms, the conductivity would be infinite. In a real lattice anharmonic motion couples the vibrations, reducing the mean free path and the lattice conductivity. Thermal conductivity is related to higher order terms in the potential and should be correlated with thermal expansion. Lattice conductivity can be viewed as the exchange of energy between high-frequency lattice vibrations, or elastic waves. A crude theory for the lattice conductivity, consistent with the Griineisen approximation, gives

$$\mathcal{K}_L = a/3\gamma^2 T K_T^{3/2} \rho^{1/2}$$

where a is the lattice parameter, γ is the Griineisen parameter, T is temperature, K_T is the isothermal bulk modulus, and p is density. This is valid for large T/θ. This relation predicts that the thermal conductivity decreases by about 20 percent as one traverses the mantle.

The contribution of "free carriers" such as electrons, holes and electron-hole pairs to thermal conduction can be estimated from the Wiedemann-Franz law relating electrical, $\mathcal{K}_e$, and thermal (lattice) conductivity. The mantle is a good electrical insulator, and the associated thermal conductivity is almost certainly negligible. The Wiedermann-Franz ratio is

$$\mathcal{K}_L/\mathcal{K}_e = (\pi^2/3)(k/e)^2 T$$

where k is Boltzmann's constant and e is the electronic charge. Using estimates of electrical conductivity, $\mathcal{K}_e$, of the mantle, we obtain estimates of thermal conductivity due to this mechanism that are some six orders of magnitude lower than observed lattice conductivities.

Excitons, or bound electron-hole pairs, may contribute to thermal conductivity at high temperature if the excitation energy is of the order of 1 eV. Evidence to date suggests a much higher energy in silicates and oxides, so exitonic thermal transport appears to be negligible in the mantle.

The thermal conductivities of various rock-forming minerals are given in Table 7-1. Note that the crust-forming minerals have about one-half to one-third of the conductivity of mantle minerals. This plus the cracks present at low crustal pressures means that a much higher thermal gradient is maintained in the crust, relative to the mantle, to sustain the same conducted heat flux. The gradient can be higher still in sediments that have conductivities of the order of 0.4 to 2×10^{-3} cal/cm s°C.

The thermal gradlient decreases with depth in the Earth because of the increasing conductivity and the decreasing amount of radioactivity-generated heat. If the crustal radioactivity and mantle heat flow are constant and the effects of temperature are ignored, regions of thick crust should have relatively high upper-mantle temperatures.

Horai and Simmons (1970) found a good correlation between seismic velocities and lattice conductivity, as expected from lattice dynamics. They found

$$V_p = 0.17\mathcal{K}_L + 5.93$$

$$V_s = 0.09\mathcal{K}_L + 3.31$$

with $\mathcal{K}_L$ in mcal/cm s°C and $V_{p,s}$ in km/s. They also found a linear relationship between the Debye temperature, 8 (in kelvins), and $\mathcal{K}_L$:

$$\theta = 25.6\mathcal{K}_L + 3.85$$

Thermal conductivity is strongly anisotropic, varying by about a factor of 2 in olivine and orthopyroxene as a function of direction. The highly conducting axes are [100] for olivine and [001] for orthopyroxene. The most conductive axis for olivine is also the direction of maximum P-velocity and one of the faster S-wave directions, whereas the most conductive axis for orthopyroxene is an intermediate axis for *P*-velocity and a fast axis for S-waves. In mantle rocks the fast P-axis of olivine tends to line up with the intermediate P-axis of orthopyroxene. These axes, in turn, tend to line up in the flow direction, which is in the horizontal plane in ophiolite sections. The vertical conductivity in such situations is much less than the average conductivity computed for mineral aggregates, which is about 7×10^{-3} cal/cm s°C at normal conditions. Conductivity decreases with temperature and may be only half this value at the base of the lithosphere. The implications of this anisotropy in thermal conductivity and the lower than average vertical conductivity have not been investigated. Two obvious implications are that the lithosphere can support a higher thermal gradient than generally supposed, giving higher upper-mantle temperatures, and that the thermal lithosphere grows less rapidly than previously calculated. For example, the thermal lithosphere at 80 Ma can be 100 km thick for $\mathcal{K} = 0.01$ cal/cm s deg and only 30 km thick if the appropriate $\mathcal{K}$ is 3×10^{-3} callcm s deg. The low lattice conductivity of the oceanic crust is usually also ignored in these calculations, but this may be counterbalanced by water circulation in the crust.

The lattice (phonon) contribution to the thermal conductivity decreases with temperature, but at high temperature radiative transfer of heat may become significant depending on the opacities of the minerals. If the opacity, ε, is independent of wavelength and temperature, then $\mathcal{K}_R$ increases strongly with temperature:

$$\mathcal{K}_R = 16n^2\sigma T^3/3\varepsilon$$

where n is the refractive index and σ is the Stefan-Boltzmann constant. If ε were constant, $\mathcal{K}_R$ would increase very rapidly with temperature and would be the dominant heat conduction mechanism in the mantle. The parameter ε^{-1} decreases from about 0.6 to 0.1 cm in the temperature range of 500 to 2000 K for olivine single crystals and approaches 0.02 cm for enstatite (Schatz and Simmons, 1972). The net result is that $\mathcal{K}_R$ is about equal to $\mathcal{K}_L$ at high temperatures and lower-mantle conditions.

Convection is the dominant mode of heat transport in the Earth's deep interior, but conduction is not irrelevant to the thermal state and history of the mantle as heat must be transported across thermal boundary layers by conduction. Thermal boundary layers exist at the surface of the Earth, at the core-mantle boundary and, possibly, at chemical interfaces internal to the mantle. Conduction is also the mechanism by which subducting slabs cool the mantle. The thicknesses and thermal time constants of boundary layers are controlled by the thermal conductivity, and these regulate the rate at which the mantle cools and the rate at which the thermal lithosphere grows.

The thermal diffusivity, κ, is defined

$$\kappa = \mathcal{K}/\rho C_v$$

and the characteristic thermal time constant of a body of dimension l is

$$\tau \approx l^2/\kappa$$

TABLE 7-1
Thermal Conductivity of Minerals

Mineral	Thermal Conductivity 10^{-3}cal/cm s°C
Albite	4.71
Anorthite	3.67
Microcline	5.90
Serpentine	7.05
Diopside	11.79
Forsterite	13.32
Bronzite	9.99
Jadeite	15.92
Grossularite	13.49
Olivine	6.7–13.6
Orthopyroxene	8.16–15.3

Horai (1971), Kobayzshigy (1974).

TABLE 7-2
Estimates of Lattice Thermal Diffusivity in the Mantle

Depth (km)	κ (cm^2/s)
50	5.9×10^{-3}
150	3.0×10^{-3}
300	2.9×10^{-3}
400	4.7×10^{-3}
650	7.5×10^{-3}
1200	7.7×10^{-3}
2400	8.1×10^{-3}
2900	8.4×10^{-3}

Horai and Simmons (1970).

The thermal diffusivities of mantle minerals are about 0.006 to 0.010 cm^2/s (see Table 7-2). In order to match the observed elevation and geoid changes across oceanic fracture zones, Crough (1979) derived a diffusivity of 0.0033 cm^2/s for the upper mantle. This low value may be related to the anisotropy discussed above or high temperatures.

Lattice Conductivity

Both thermal conductivity and thermal expansion depend on the anharmonicity of the interatomic potential and therefore on dimensionless measures of anharmonicity such as γ or $\alpha\gamma T$.

The lattice or phonon conductivity, $\mathcal{K}_L$, is

$$\mathcal{K}_L = \frac{1}{3} C_V \bar{V} l$$

where $\bar{V}$ is the mean sound velocity, l is the mean free path,

$$l = a/\alpha\gamma T = aK_T/\rho C_V \gamma^2 T$$

and a is the interatomic distance, and K_T is the isothermal bulk modulus. Therefore,

$$\mathcal{K}_L = (1/3)\bar{V} a K_T/\rho\gamma^2 T$$
$$= (1/3)\left(\frac{1}{V_p^3} + \frac{2}{V_s^3}\right)^{-1/3} aK_T/\rho\gamma^2 T$$

This gives

$$\frac{\partial \ln \mathcal{K}_L}{\partial \ln \rho} = \frac{\partial \ln K_T}{\partial \ln \rho} - 2\frac{\partial \ln \gamma}{\partial \ln \rho} + \gamma - \frac{4}{3}$$

where we have used the approximation

$$\partial \ln \bar{V}/\partial \ln \rho \simeq \gamma$$

For lower-mantle properties this expression is dominated by the $\partial \ln K_T/\partial \ln \rho$ term, and the variation of $\mathcal{K}_L$ is similar to the variation of K_T.

The lattice conductivity decreases approximately linearly with temperature, a well-known result, but increases rapidly with density. The temperature effect dominates in the shallow mantle, giving a decreasing $\mathcal{K}_L$, but pressure causes $\mathcal{K}_L$ to be high in the lower mantle. This has important implications regarding the properties of thermal boundary layers, the ability of the lower mantle to conduct heat from the core and into the upper mantle, and the convective mode of the lower mantle.

The general correlation of $\mathcal{K}_L$ with the elastic wave velocities suggests that pressure-induced phase changes in the transition region and lower mantle will also increase the lattice conductivity. Thermally induced velocity variations in deep slabs will be small because of the high $\mathcal{K}_L$ and low temperature derivatives of velocity. The expected increase of $\mathcal{K}_L$ with compression, with bulk modulus, with sound speed and across low pressure–high pressure phase changes has been verified by experiment (Fujisawa and others, 1968) as has the correlation of $\mathcal{K}_L$ with elastic wave velocities. We expect about a factor of 3 increase in $\mathcal{K}_L$, caused by the increase in seismic velocities, from shallow-mantle to transition-zone pressures. The erroneous use of an olivine-like $\mathcal{K}_L$ for the deep slab and a $(\partial V_P/\partial T)_P$ of about twice that of olivine (Creager and Jordan, 1984) are partly responsible for the conclusion about the persistence and extent of deep slab-related seismic anomalies. On the other hand, changes in mineralogy associated with solid-solid phase changes are much more important than temperature.

The ratio $\alpha/\mathcal{K}_L$ decreases rapidly with depth in the mantle, thereby decreasing the Rayleigh number. Pressure also increases the viscosity, an effect that further decreases the Rayleigh number of the lower mantle. The net effect of these pressure-induced changes in physical properties is to make convection more sluggish in the lower mantle, to decrease thermal-induced buoyancy and to increase the thickness of the thermal boundary layer in D", above the core-mantle boundary.

The thermal conductivity of crystals is a complex subject even when many approximations and simplifying assumptions are made. The mechanism for transfer of thermal energy is generally well understood in terms of lattice vibrations, or high-frequency sound waves. This is not enough, however, since thermal conductivity would be infinite in an ideal harmonic crystal. We must understand, in addition, the mechanisms for scattering thermal energy and for redistributing the energy among the modes and frequencies in a crystal so that thermal equilibrium can prevail. An understanding of thermal "resistivity," therefore, requires an understanding of higher order effects, including anharmonicity.

High-frequency elastic energy is scattered by imperfections such as point defects, dislocations, grain boundaries and impurities, including isotopic differences, and nonlinearity or anharmonicity or interatomic forces. The latter effects can be viewed as nonlinear interactions of the thermal sound waves themselves, a sort of self-scattering.

The parameters that enter into a theory of lattice conductivity are fairly obvious. One expects that the temperature, specific heat and the coefficient of thermal expansion will be involved. One expects that some measure of anharmonicity, such as y, will be involved. In addition one needs a measure of a mean free path or a mean collision time or a measure of the strength and distribution of scatterers. The velocities of the sound waves and the interatomic distances are also likely to be involved.

Debye (1912) explained the thermal conductivity of dielectric or insulating solids in the following way. The lattice vibrations can be resolved into traveling waves that carry heat. Because of anharmonicities the thermal fluctuations in density lead to local fluctuations in the velocity of lattice waves, which are therefore scattered. Simple lattice theory provides estimates of specific heat and sound velocity and how they vary with temperature and volume. The theory of attenuation of lattice waves involves an understanding of how thermal equilibrium is attained and how momentum is transferred among lattice vibrations.

The heat flow, Q, associated with a given mode type (longitudinal or transverse) can be written in terms of the energy, wave number and group velocity of the mode.

The distinction between group velocity, $\mathbf{v}, = \partial\omega/\partial\mathbf{k}$, and phase velocity, $\omega/\mathbf{k}$, is seldom made in the theory because dispersion is generally ignored. If ω is proportional to the wave number, k, then $\mathbf{v}$ is constant and phase and group velocities are equal. This assumption breaks down for high frequencies or large k. At high frequencies $\mathbf{v}$, becomes very small, and high frequencies therefore are not efficient in transporting heat. High-frequency waves are those having wavelengths comparable to a lattice spacing.

Because of the discreteness of a lattice, the possible energy levels are quantized. We can treat the thermal properties of a lattice as a gas of phonons. **A** quantum of lattice vibration is called a phonon and acts as a particle of energy $\hbar\omega$, momentum $\hbar\mathbf{k}$ and velocity $\partial\omega/\partial\mathbf{k}$. There is no limit to the number of quanta in a normal mode. The phonons carry a heat current, which is the sum of the heat currents carried by all normal modes:

$$Q = \sum_{\mathbf{k}} N(\mathbf{k})\hbar\omega\ \partial\omega/\partial\mathbf{k}$$

The lattice conductivity is a sum over all wave types of the integral over all wave numbers

$$\mathcal{K}_L = \frac{1}{3}\sum_j \int d\mathbf{k}\mathbf{v}_j^2(\mathbf{k})\tau_j(\mathbf{k})C_V\mathbf{v}_j(\mathbf{k})$$

where $\mathbf{v}$, is the group velocity of the jth wave type and τ_j is the lifetime or collision time of this wave type.

The thermal resistance is the result of interchange of energy between lattice waves, that is, scattering. Scattering can be caused by static imperfections and anharmonicity. Static imperfections include grain boundaries, vacancies, interstitials and dislocations and their associated strain fields, which considerably broadens the defects cross-section. These "static" mechanisms generally become less important at high temperature. Elastic strains in the crystal scatter because of the strain dependence of the elastic properties, a nonlinear or anharmonic effect. An elastic strain alters the frequencies of the lattice waves.

DIFFUSION AND VISCOSITY

Diffusion and viscosity are activated processes and depend more strongly on temperature and pressure than the properties discussed up to now. The diffusion of atoms, the mobility of defects, the creep of the mantle and seismic wave attenuation are all controlled by the diffusivity.

$$D(P,T) = \zeta a^2 \nu \exp[-G^*(P,T)/RT]$$

where G^* is the Gibbs free energy of activation, ζ is a geometric factor and ν is the attempt frequency (an atomic vibrational frequency). The Gibbs free energy is

$$G^* = E^* + PV^* - TS^*$$

where E*, V^* and S^* are activation energy, volume and entropy, respectively. The diffusivity can therefore be written

$$D = D_o \exp -(E^* + PV^*)/RT$$

$$D_o = \zeta a^2 \nu \exp S^*/RT$$

where S^* is generally in the range R to SR. The theory for the volume dependence of D_o is similar to that for thermal diffusivity, $\kappa = \mathcal{K}_L/\rho C_V$. It increases with depth but the variation is small, perhaps an order of magnitude, compared to the effect of the exponential term. The product of $\mathcal{K}_L$ times viscosity is involved in the Rayleigh number, and the above considerations show that the temperature and pressure dependence of this product depend mainly on the exponential terms.

The activation parameters are related to the derivative of the rigidity (Keyes, 1963):

$$V^*/G^* = (1/K_T)\left[\left(\frac{\partial \ln G}{\partial \ln \rho}\right)_T - 1\right]$$

The effect of pressure on D can be written

$$-\frac{RT}{K_T}\left(\frac{\partial \ln D}{\partial \ln \rho}\right)_T = V^* = \frac{1}{K_T}\left[\left(\frac{\partial \ln G}{\partial \ln \rho}\right)_T - 1\right]G^*$$

or

$$\left(\frac{\partial \ln D}{\partial \ln \rho}\right)_T = -\frac{G^*}{RT}\left[\left(\frac{\partial \ln G}{\partial \ln \rho}\right)_T - 1\right]$$

For a typical value of 30 for G^*/RT we have V* decreasing from 4.3 to 2.3 cm³/mole with depth in the lower mantle, using elastic properties from the PREM Earth model. We also have

$$-(\partial \ln D/\partial \ln p), \approx 48 \text{ to } 40$$

This gives a decrease in diffusivity, and an increase in viscosity, of about a factor of 60 to 80, due to compression, across the lower mantle. In convection calculations and geoid modeling it is common practice to assume a constant viscosity for the lower mantle. This is a poor assumption.

Viscosity

A general expression for viscosity, η, is

$$\eta \approx (G/\sigma)^n$$

where n is a constant generally between 1 and 3 and σ is the nonhydrostatic stress. This gives an additional increase of viscosity over that contributed by the diffusivity, D, unless σ decreases rapidly with depth. The general tendency of η to increase with depth may be reversed in the D" zone due to a high thermal gradient and, possibly, an increase in σ. The decrease in V* with depth also means that compression-induced viscosity increases will be milder at the base of the mantle. A low-viscosity D" layer could reduce the ability of mantle convection to deform the core-mantle boundary.

The change in viscosity across a chemical or phase boundary is not easily determined. The pre-exponential term in the diffusivity will increase across a boundary that involves an increase in bulk modulus and mean sound velocity, or Debye frequency. Therefore, the viscosity will ***decrease*** due to this factor. For the same reason lattice conductivity and the thermal diffusivity will increase. The activation volume of the low-density phase will generally be greater than that of the high-density phase. This means that the viscosity jump across a deep boundary will be negative if both phases had the same viscosity at zero pressure. The high temperature gradient in thermal boundary layers, such as D", the lithosphere and, possibly, near the 650-km discontinuity will cause the diffusivity to increase. Therefore, viscosities will tend to ***decrease*** across mantle discontinuities unless the activation energies are sufficiently lower for the dense phases that the geothermal gradient can overcome the above effects or unless pre-exponential, crystal structure, defect or nonhydrostatic stress considerations play an appropriate role.

The combination of physical parameters that enters into the Rayleigh number, $\alpha/\kappa\eta$ (coefficient of expansion a, thermal diffusivity κ, and viscosity η), decreases rapidly with compression. The decrease through the mantle is of the order of 10^6 to 10^7. With parameters appropriate for the mantle, the increase due to temperature is of the order of 10^6. Therefore, there is a delicate balance between temperature and pressure. The local Rayleigh number in thermal boundary layers increases because of the dominance of the thermal gradient over the pressure gradient.

Diffusion

Diffusion of atoms is important in a large number of geochemical and geophysical problems: metamorphism, element partitioning, creep, attenuation of seismic waves, electrical conductivity and viscosity of the mantle. Diffusion means a local nonconvective flux of matter under the action of a chemical or electrochemical potential gradient.

The net flux J of atoms of one species in a solid is related to the gradient of the concentration, N, of this species

$$J = -D \text{ grad N}$$

where D is the diffusion constant or diffusivity and has the same dimensions as the thermal diffusivity. This is known as Fick's law and is analogous to the heat conduction equation.

Usually the diffusion process requires that an atom, in changing position, surmount a potential energy barrier. If the barrier is of height G*, the atom will have sufficient energy to pass over the barrier only a fraction exp(−G*/RT) of the time. The frequency of successes is therefore

$$\nu = \nu_o \exp(-G^*/RT)$$

where ν_o is the attempt frequency, usually taken as the atomic vibration, or Debye, frequency, which is of the order of 10^{14} Hz. The diffusivity can then be written

$$D = \zeta \nu a^2$$

where ζ is a geometric factor that depends on crystal structure or coordination and that gives the jump probability in the desired direction and a is the jump distance or interatomic spacing.

The factor ν takes into account the fact that if an atom can jump equally in m directions ($m = 6$ in a face-centered cubic lattice, for example), then the distance moved in the desired direction is different for each jump direction. Also, the atom can only jump to empty sites, that is, vacancies. The probability for this is C_v, the vacancy concentration, where

$$C_v = e^{-G_v^*/RT}$$

where G_v^* is the free energy of formation of a vacancy.

Diffusion, like most thermally activated processes, exhibits a change in activation energy between high-temperature and low-temperature regimes. ***At*** low temperatures the number of diffusing ions is independent of temperature, and therefore the energy of formation is not involved. This is the extrinsic range of temperature. Diffusion proceeds via chemical vacancies due to non-stoichiometry or impurities, which outnumber the thermally generated vacancies. At

high temperature thermally generated vacancies are produced, and the energy of formation is also involved. The transition from the extrinsic to the intrinsic regime usually occurs at about 0.8 of the melting temperature. The barrier to extrinsic diffusion, G_x^*, is the maximum change in free energy due to the lattice distortion associated with the motion of the ion from its lattice site into a neighboring vacancy. D_o is generally greater than 1 cm^2/s for intrinsic diffusion and much less than 1 cm^2/s in the extrinsic range.

Motion of vacancies (Schottky defects) and interstitials (Frenkel defects) are important in ionic conductivity. The ionic conductivity is given by

$$\sigma = (N_o e^2 p \nu a^2/kT) e^{-E/kT}$$

where N_o is the total number of ions of the appropriate species per unit volume and p is the fraction of ions able to move.

The frequency factor ν and the activation energy can be found from diffusion experiments. They can also be found from dynamic experiments such as anelastic or attenuation measurements involving elastic waves. An absorption peak, for example, occurs when $\omega/\nu = 1$ or $\omega\tau = 1$. The activation energy is found from the shift in the absorption peak with temperature. Generally, solids exhibit a series of absorption peaks, one for each physical mechanism or diffusing species. The theories of creep, or mantle viscosity, and seismic wave attenuation are intimately related to theories of diffusion. For a mechanism to be important at seismic frequencies and mantle temperatures, the frequency factor ν must be close to the seismic frequency w. ν can be estimated from ν_o and G*, given the temperature, pressure, and atomic species. The diffusive properties of the common rock-forming elements (Mg, Fe, Ca, Al, Si and O) are of most relevance in studies of mantle creep and attenuation. Experimentally determined diffusion parameters in various oxides and silicates are given in Table 7-3 and 7-4. E* is generally well determined if the temperature range is extensive enough, but D_o requires a long extrapolation. In curve-fitting diffusion data there is a trade-off between D_o and E*.

Regions of lattice imperfections in a solid are regions of increased mobility. Dislocations are therefore high-mobility paths for diffusing species. The rate of diffusion in these regions can exceed the rate of volume or lattice diffusion. In general, the activation energy for volume diffusion is higher than for other diffusion mechanisms. At high temperature, therefore, volume diffusion can be important. In and near grain boundaries and surfaces, the jump frequencies and diffusivities are also high. The activation energy for surface diffusion is related to the enthalpy of vaporization.

The effect of pressure on diffusion is given by the activation volume, V*:

$$V^* = RT(\partial \ln D/\partial P)_T - RT\left(\frac{\partial \ln \zeta a^2 \nu}{\partial P}\right)_T$$

TABLE 7-3
Diffusion in Silicate Minerals

Mineral	Diffusing Species	T (K)	D (m^2/s)
Forsterite	Mg	298	2×10^{-18}
	Si	298	10^{-19}–10^{-21}
	O	1273	2×10^{-20}
Zn_2SiO_4	Zn	1582	3.6×10^{-15}
Zircon	O	1553	1.4×10^{-19}
Enstatite	Mg	298	10^{-20}–10^{-21}
	O	1553	6×10^{-16}
	Si	298	6.3×10^{-22}
Diopside	Al	1513	6×10^{-16}
	Ca	1573	1.5×10^{-15}
	O	1553	2.4×10^{-16}
Albite	Ca	523	10^{-14}
	Na	868	8×10^{-17}
Orthoclase	Na	1123	5×10^{-15}
	O	~1000	10^{-20}

Freer (1981).

The second term can be estimated from lattice dynamics and pressure dependence of the lattice constant and elastic moduli. This term is generally small. V* is usually of the order of the atomic volume of the diffusing species. The activation volume is also made up of two parts, the formational part V_f^* and the migrational part V_m^*. Ordinarily the temperature and pressure dependence of a and ν are small.

For a vacancy mechanism V_f^* is simply the atomic volume since a vacancy is formed by removing an atom. This holds if there is no relaxation of the crystal about the vacancy. Inevitably there must be some relaxation of neighboring atoms inward about a vacancy and outward about an interstitial, but these effects are small. In order to move, an atom must squeeze through the lattice, and V_m^* can also be expected to about an atomic volume.

The work performed in creating a lattice imperfection can be estimated from elasticity theory if the lattice can be treated as a continuum. In this case

$$V^*/G^* = -[(\partial \ln G/\partial \ln V)_T - 1]K_T^{-1} = [1 + \{G\}_T]K_T^{-1}$$

where G is the shear modulus and K_T is the isothermal bulk modulus (Keyes, 1963). The magnitude of $\{G\}_T$, from the previous chapter, is about 3. The Grüneisen assumption, that all vibrational frequencies of the lattice depend on volume in the same way, gives

$$(\partial \ln K/\partial \ln V)_T = -(2\gamma + 1/3) = (\partial \ln G/\partial \ln V)_T$$

and

$$V^*/G^* = 2(\gamma - 1/3)K_T^{-1}$$

Borelius (1960) obtained a similar expression, but a smaller effect, by assuming that the increase in volume dur-

ing the self-diffusion act is equal to the volume of the hard atomic core:

$$V^*/G^* = -1/3(K_T)^{-1}(\partial \ln K_T/\partial \ln V), = \{K_T\}_T/3K_T$$

The activation entropy S* can also be estimated from a strain energy model (Keyes, 1960):

$$S^*/G^* = -\alpha[(\partial \ln G/\partial \ln V), + 1]$$
$$= \alpha[\{G\}_P - 1]$$

or

$$V^*/S^* = (\alpha K_T)^{-1}[(\text{d-ln } G/\partial \text{ ln } V)_T + 1]$$
$$\div [(\partial \ln G/\partial \ln V), + 1]$$
$$= (1 - \{G\}_T)/\alpha K_T(1 - \{G\}_P)$$

With the Griineisen assumption, that the rigidity G depends on temperature and pressure only through the volume,

$$V^*/S^* \approx (\alpha K_T)^{-1}$$

and

$$S^* = 2(\gamma - 1/3)\alpha G^*$$

Some of these approximations are not necessary for upper-mantle minerals since $(\ln G/\partial \ln V), = \{G\}_T$ and $(\partial \ln G/\partial \ln V), = \{G\}$, are both known.

Sammis and others (1977) estimated values for V* of about 8 to 12 cm^3/mole for oxygen self-diffusion in olivine and about 3 to 5 cm^3/mole in the lower mantle, decreasing with depth. Another estimate for activation volume of about 2 cm^3/mole for the lower mantle was based on seismic attenuation data (Anderson, 1967). Of course the V^* for attenuation may differ from the V* for creep since different diffusing species may be involved. Nevertheless, the effect of pressure on ionic volumes leads one to expect that V* will decrease with depth and, therefore, that activated processes became less sensitive to pressure at high pressure. Indeed, both viscosity and seismic factor Q do not appear to increase rapidly with depth in the lower mantle.

TABLE 7-4
Diffusion Parameters in Silicate Minerals

Mineral	Diffusing Species	D_o (m^2/s)	Q (kJ mol^{-1})
Olivine	Mg	4.1×10^{-4}	373
	Fe	4.2×10^{-10}	162
	O	5.9×10^{-8}	378
	Si	7.0×10^{-13}	173
	Fe-Mg	6.3×10^{-7}	239
Garnet	Sm	2.6×10^{-12}	140
	Fe-Mg	6.1×10^{-4}	344
Ca_2SiO_4	Ca	2.0×10^{-6}	230
$CaSiO_3$	Ca	7	468
Albite	Na	1.2×10^{-7}	149
	O	1.1×10^{-9}	140
Orthoclase	Na	8.9×10^{-4}	220
	O	4.5×10^{-12}	107
Nepheline	Na	1.2×10^{-6}	142
Glass			
Albite	Ca	3.1×10^{-5}	193
Orthoclase	Ca	2.6×10^{-6}	179
Basalt	Ca	4.0×10^{-5}	209
	Na	5×10^{-10}	41.8

Freer (1981).

HOMOLOGOUS TEMPERATURE

The ratio E^*/T_m is nearly constant for a variety of materials, though there is some dependence on valency and crystal structure. Thus, the factor E^*/T in the exponent for activated processes can be written $\lambda T_m/T$ where λ is roughly a constant and T_m is the "melting temperature." If this relation is assumed to hold at high pressure, then the effect of pressure on G*, that is, the activation volume V*, can be estimated from the effect of pressure on the melting point:

$$D(P,T) = D_o \exp[-\lambda T_m(P)/RT]$$

and

$$V^* = E^* \frac{dT_m}{dP} \Big/ T_m$$

which, invoking the Lindemann law, becomes

$$V^* = 2E^*(\gamma - 1/3)/K_T$$

which is similar to expressions given in the previous section. The temperature T, normalized by the "melting temperature," T_m, is known as the homologous temperature. It is often assumed that activated properties depend only on TIT, and that the effect of pressure on these properties can be estimated from $T_m(P)$.

The melting point of a solid is related to the equilibrium between the solid and its melt and not to the properties of the solid alone. Various theories of melting have been proposed that involve lattice instabilities, critical vacancy concentrations or dislocation densities, or amplitudes of atomic motions. These are not true theories of melting since they ignore the properties of the melt phase, which must be in equilibrium with the solid at the melting point.

DISLOCATIONS

Dislocations are extended imperfections in the crystal lattice and occur in most natural crystals. They can result from the crystal growth process itself or by deformation of the

crystal. They can be partially removed by annealing. Although dislocations occur in many complex forms, all can be obtained by the superposition of two basic types: the edge dislocation and the screw dislocation. These can be visualized by imagining a cut made along the axis of a cylinder, extending from the edge to the center and then shearing the cylinder so the material on the cut slides radially (edge dislocation) or longitudinally (screw dislocation). In the latter case the cylinder is subjected to a torque.

The first suggestion of dislocations was provided by observations in the nineteenth century that the plastic deformation of metals proceeded by the formation of slip bands wherein one portion of a specimen sheared with respect to another. Later the theory evolved that real crystals were composed of small crystallites, slightly misoriented with respect to one another, whose boundaries consist of arrays of dislocation lines. Theories of crystallization involve the nucleation of atoms on the ledges formed by the emergence of a dislocation at the surface of a crystal. The rapid equilibration of point defects in a crystal also involves dislocations as sources and sinks of point defects in crystals. This is also involved in diffusional and dislocation models of creep of solids.

The major impetus for the development of dislocation theory involved the consideration of the strength of a perfect crystal. The theoretical shear strength of a crystal is

$$\text{Strength} = Gb/2\pi a \approx G/5$$

where G is rigidity, b, the Burger's vector, is the magnitude of a simple lattice-translation and a is the spacing of atomic planes. The shear stress required to initiate plastic flow in metals, however, is only about 10^{-3} to 10^{-4} G. This was resolved by the introduction of lines of mismatch, or dislocations, in the lattice of crystals. Slip could then proceed by the unzippering effect of a dislocation line moving through the lattice. Work by Orowan, Polanyi, Taylor and Burgess in the 1930s to resolve the strength problem led to the development of modern dislocation theory. The theory was well developed and dislocations were almost completely understood before they were even actually observed.

An elementary property of a dislocation is the Burger's vector b. If a closed circuit is made by proceeding from one atom to another in a perfect crystal and then the same circuit is made in a part of a crystal that contains a dislocation, there will be closure error in the latter case. This closure error or closure vector is the Burger's vector and is roughly one interatomic spacing.

Consider a crystal that contains a half-cut and then is subjected to shear that displaces atoms on opposite sides of the cut by a single lattice spacing. The cut defines the slip plane, and the dislocation line, the edge of the cut, marks the boundary between the slipped and unslipped parts of the crystal. The displacement is specified by the slip or Burger's vector. Since b is a lattice vector, the atoms on opposite sides of the slip plane remain in alignment; thus the slip plane is not a discontinuity in the crystal, but there is distortion of the crystal around the dislocation line. The energy of a dislocation is proportional to b^2, so crystals tend to deform by slip with b the smallest lattice vector. The vector b is normal to the dislocation line for an edge dislocation and parallel to the dislocation line for a screw dislocation.

Dislocations can contribute to creep by climb or by glide. Dislocation climb involves the lengthening or shortening of the extra plane of atoms defining the dislocation. Dislocation glide, or slip, involves the transfer of an edge dislocation to an adjacent plane of atoms.

DISLOCATION CREEP

Creep in mantle silicates can occur by motions of vacancies by the self-diffusion mechanism (Nabarro-Herring creep) or by the motion of dislocations. The respective strain rates are

$$\dot{\varepsilon}_{NH} = K_1(D/l^2)(\sigma\Omega/kT)$$

and

$$\dot{\varepsilon}_D = K_2(D/b^2)(G\Omega/kT)(\sigma/G)^3$$

where l is the grain size, Ω the atomic volume, D the diffusivity, b the length of the Burger's vector of the dislocation, σ the shear stress, G the rigidity, and K_1 and K_2 are dimensionless constants. The second mechanism, called power-law creep, is commonly observed in mantle silicates at high temperature. Diffusional creep can be more important at low stress and small grain size as small grains, or subgrains, place the sources and sinks of vacancies closer together. Note that $\dot{\varepsilon}_{NH}$ depends linearly on σ and is therefore Newtonian. Power-law creep, & is distinctly non-Newtonian.

If diffusion is preferentially along grain boundaries we have Coble creep,

$$\dot{\varepsilon}_C = K_1(D/l^2)(\alpha\Omega/kT)[1 + (\pi\delta/l)](D_B/D)$$

where δ is the thickness of the grain boundary ($\sim 200b$) and D_B is the grain boundary diffusivity.

Note that all these expressions contain D and therefore have the same temperature and pressure dependence as the appropriate diffusing species, presumably Si or O.

It is probable that steady-state creep in the mantle is controlled by dislocation climb and is therefore limited by the slow process of self-diffusion and, possibly, jog formation on dislocation lines. There is abundant evidence that mantle minerals contain many dislocations; most are probably associated with cell walls of subgrains. Under large stresses dislocation multiplication can take place.

The average subgrain size, L, and dislocation density, ρ_m, are observed to be related to the stress σ (Nicolas and Poirer, 1976)

$$Llb \approx G/\sigma$$

$$b^2\rho_m \approx (\sigma/G)^2$$

These relations can be used to estimate the stress in the mantle from studies of crystals derived from the mantle. These relations lead to

$$b^2\rho_m = K^2(b/L)^2$$

where the constant K is about 10 for laboratory-deformed olivine (Gittus, 1976). The creep rate can be written

$$\dot{\varepsilon} = \sigma/\tau G$$

where τ is a characteristic time often called the Maxwell time.

For diffusional creep, with stress-dependent grain or subgrain dimensions,

$$\tau = K_2(G/\sigma)^2 \frac{kTb^2 \exp E^*/RT}{GD_o\Omega}$$

where it is assumed that cell walls are efficient sources and sinks of vacancies. This differs from the usual equation for diffusional creep because of the stress dependence of the grain size. K_2 is about 20 (Minster and Anderson, 1981).

For dislocation creep the strain rate is

$$\dot{\varepsilon} = \rho_m \frac{b\Lambda}{d} V$$

where A is the mean free path of the dislocation and d is the distance covered at the rate-controlling speed V, usually the climb velocity. For this case

$$\tau = K_3(G/\sigma)^2 \frac{kTb^2 \exp E^*/RT}{GD_o\Omega_v}$$

where K_3 is roughly 1 and Ω_v is the volume of a vacancy.

For a polygonized network of dislocations, the climb of dislocations in cell walls is rate-limiting, but the characteristic time for creep involves both the motion of the long mobile dislocations in the cells and the shorter dislocations in the walls. Dislocations sweep across the grain, under the action of an imposed stress, and then climb and are annihilated in cell walls or grain boundaries. The Maxwell time for this mechanism is

$$\tau = (3/K^4)(G/\sigma)^2 \frac{kTb^2 \exp [(E_s^* + E_j)/RT]}{GD_o\Omega_v}$$

where K is a constant of order 10 to 50 ($\sim L\sigma/Gb$), E_s^* is the self-diffusion energy and E_j is the jog formation energy, of order 17 to 58 kcal/mole for olivine. This can be termed the cell-wall recovery model, which was formulated by Gittus (1976) and discussed by Minster and Anderson (1980, 1981). This is an efficient mechanism because of the low τ and, at high temperature, because of the high activation energy.

The dominant creep mechanism depends on such parameters as grain size, temperature, pressure and stress level. It may therefore be different in the Earth than in the laboratory. Laboratory results are generally obtained at high stress levels, high strain rates and short times. Results cannot necessarily be extrapolated to low stresses and low strain rates and, even if they can, other mechanisms may become more effective.

The low-stress creep data for olivine can support either an $\dot{\varepsilon} \approx \sigma^3$ or σ^2 interpretation, but measurements on individual samples support the high exponent. The difference can result in a several order of magnitude variation in the extrapolated creep rate at important geophysical stress levels of about 10 bars. Estimated values of τ at 10 bars are 10^{-11} to 5×10^{-10} s for a σ^3 law and 2×10^{-13} to 10^{-11} s for a σ^2 law.

These values for τ_o, and the associated activation energy E*, rule out diffusional creep, involving self-diffusion of oxygen and silicon, as a mechanism to explain laboratory creep in olivine. Several other proposed mechanisms for creep can also be ruled out by this procedure. Minster and Anderson (1981) concluded that a dislocation model that involves cell-wall recovery under self-stress and silicon diffusion satisfies the olivine creep data and might therefore be an appropriate creep mechanism for the mantle. Theoretical Maxwell times, appropriate for mantle conditions, are shown in Figure 7-1.

Estimated activation volumes for O and Si diffusion in olivine are about 11 cm³/mole and 4 cm³/mole, respectively, which can be compared with the estimates from seismic data indicating a decrease from 11 to 6 cm³/mole in the upper mantle and 6 to 3 cm³/mole in the lower mantle (Anderson, 1967; Sammis and others, 1977). These considerations limit the total variation of viscosity in the mantle to about two orders of magnitude, assuming no change in the pre-exponential term.

Strain rate, 8, and effective viscosity, η, are related to the characteristic time by

$$\tau = \sigma/G\dot{\varepsilon} = \eta/G$$

and therefore the viscosity can be calculated from the expressions given above. The expression for viscosity for the dislocation cell-wall recovery model is

$$\eta = (3/K^4)(G/\sigma)^2 \frac{kTb^2 \exp E^*/RT}{D_o\Omega_v}$$

where

$$E^* = E_s^* + E_j - \Delta E^*/2$$

where E_s^* is the activation energy for self-diffusion of the slowest moving species (presumably oxygen or silicon), E_j is the jog formation energy and AE* is the difference between the activation energies for bulk diffusion and core diffusion, to be taken into account when E_j exceeds $\Delta E^*/2$. The ΔE^* term is only involved if dislocation core diffusion is important and there are few geometric jogs in the wall dislocations.

Figure 7-2 shows creep data for olivine. The parameter

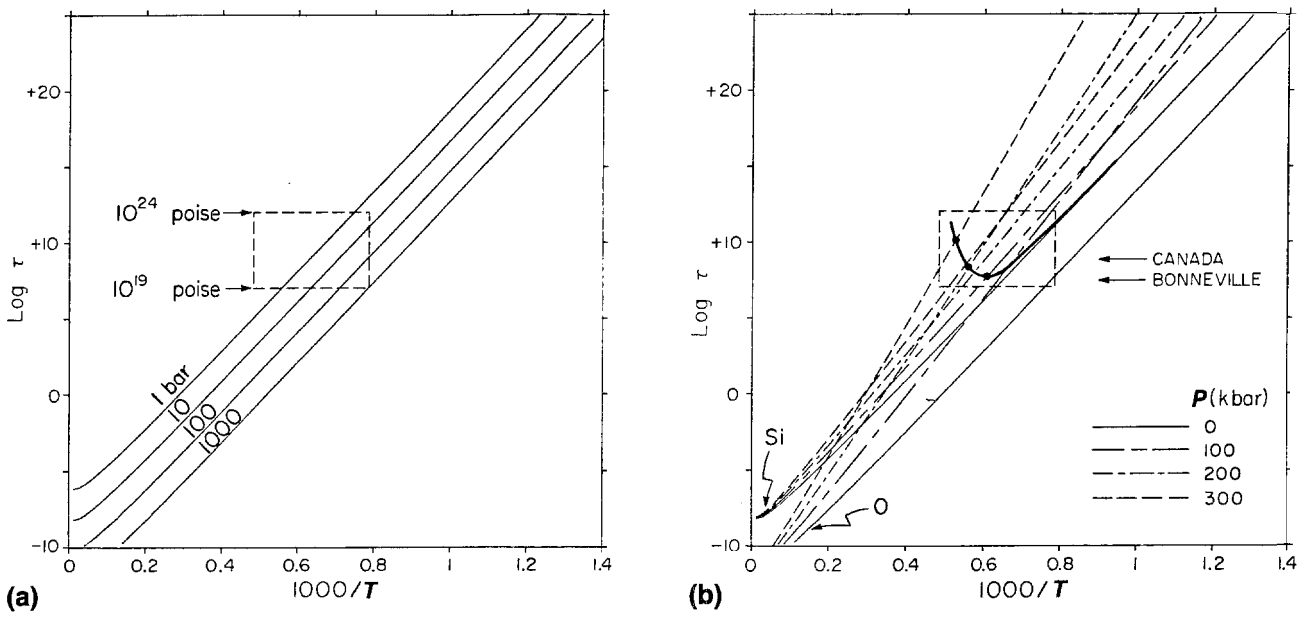

FIGURE 7-1
(a) Temperature dependence of Maxwell time τ for several values of applied load, for a creep model that satisfies laboratory observations with a σ^3 interpretation (after Minster and Anderson, 1981). **(b)** Effect of confining pressure on Maxwell times τ. At pressures greater than 200 kbar, oxygen diffusion becomes slower and controls self-diffusion. Simple thermal model of the mantle (heavy line) is compared with Crough's (1977) estimates for isostatic rebound for Lake Bonneville and the Canadian shield (after Minster and Anderson, 1981).

K is the ratio of cell diameter to the average dislocation length, including mobile and cell-wall dislocations.

Steady-state creep data for olivine for stresses between several hundred bars and several kilobars are well fit by a dislocation climb model where the strain rate is proportional to the third power of the stress (Goetze and Kohlstedt, 1973). At lower stresses the data deviate from this relationship and approach a stress-squared dependency.

THE LITHOSPHERE

The lithosphere is the cold outer shell of the Earth, which can support stresses elastically. There has been much confusion regarding the thickness of the lithosphere because the roles of time and stress have not been fully appreciated. Since mantle silicates can flow readily at high temperatures and flow more rapidly at high stresses, the lithosphere appears to be thicker at low stress levels and short times than it does for high stress levels and long times. Thus, the elastic lithosphere is thick when measured by seismic or postglacial-rebound techniques. At longer times the lower part of the instantaneous elastic lithosphere relaxes and the effective elastic thickness decreases. Thus, the elastic lithosphere is relatively thin for long-lived loads such as seamounts and topography. Estimates of the flexural thickness of the lithosphere range from 10 to 35 km for loads having durations of millions of years. The elastic lithosphere can be expected to be much thicker for short-duration loads such as ice caps. A more complete definition of the lithosphere is that part of the crust and upper mantle that deforms elastically for the load and time scale in question.

In theoretical discussions of the lithosphere, it is usually assumed that the viscosity or creep resistance of the

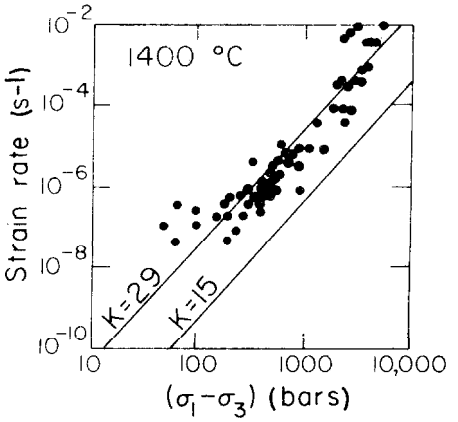

FIGURE 7-2
Strain rate versus stress difference data for olivine at 1400°C compared with the theory for two subgrain sizes (after Minster and Anderson, 1981). Data from Kohlstedt and Goetz (1974).

mantle depends only on temperature, pressure and stress. The oceanic lithosphere, in this framework, thickens with time only because it is cooling, and the thickness can be related to the depth of a given isotherm. The viscosity, or strength, of the mantle depends also on composition, mineralogy and crystal orientation. If the upper mantle is layered, then the lithosphere-asthenosphere boundary may be controlled by factors other than temperature. For example, if the subcrustal layer is olivine-rich harzburgite, it may be stronger at a given temperature than a clinopyroxene-garnet-rich layer, which has been postulated to occur at greater depth in the oceanic mantle. If the latter is weak enough, the lithosphere-asthenosphere boundary may represent a chemical boundary rather than an isotherm. Likewise, a change in the preferred orientation of the dominant crystalline species may also markedly affect the creep resistance.

The layer that translates coherently, the "plate" of plate tectonics, is often taken to be identical with the elastic lithosphere. This is probably a valid approximation if the stresses and time scales of the experiment that is used to define the flexural thickness are similar to the stresses and time scales of plate tectonics. It must be kept in mind, however, that mantle silicates are anisotropic in their flow characteristics, and that the stresses involved in plate tectonics may have different orientations than the stresses involved in surface loading experiments.

In a convecting mantle there is a thermal boundary layer through which heat must pass by conduction. The thickness of the thermal boundary layer is controlled by such parameters as conductivity and heat flow and is related in a simple way to the thickness of the elastic layer. Since temperature increases rapidly with depth in the conduction layer, and viscosity decreases rapidly with temperature, the lower part of the boundary layer probably lies below the elastic lithosphere; that is, only the upper part of the thermal boundary layer can support large and long-lived elastic stresses. Unfortunately, the conduction layer too is often referred to as the lithosphere.

Most recent models of the Earth's mantle have an upper-mantle low-velocity zone, LVZ, overlain by a layer of higher velocities, referred to as the LID (see Chapter **3).** The LID is also often referred to as the lithosphere. Seismic stresses and periods are, of course, much smaller than stresses and periods of geological interest. If seismic waves measure the relaxed modulus in the LVZ and the high-frequency or unrelaxed modulus in the LID, then, in a chemically homogeneous mantle, the LID should be much thicker than the elastic lithosphere. If the LID is chemically distinct from the LVZ, then one might also expect a change in the long-term rheological behavior at the interface. If the LID and the elastic lithosphere turn out to have the same thickness, then this would be an argument for chemical or crystallographic rather than thermal control of the mechanical properties of the upper mantle.

In summary, we recognize the following "lithospheres":

1. The elastic, flexural or rheological lithosphere. This is the closest to the classical definition of a rocky, or strong, outer shell. It can be defined as that part of the crust and upper mantle that supports elastic stresses of a given size for a given period of time. The thickness of this lithosphere depends on the stress and time.
2. The plate. This is that part of the crust and upper mantle that translates coherently in the course of plate tectonics. The thickness of the plate may be controlled by chemical or buoyancy considerations or by stress, as well as by temperature.
3. The chemical lithosphere. The density and mechanical properties of the lithosphere are controlled by chemical composition and crystal structure as well as temperature. If chemistry and mineralogy dominate, then the elastic lithosphere and LID may be identical. If the lithosphere, below the crust, is mainly depleted peridotite or harzburgite, it may be buoyant relative to the underlying mantle.
4. The thermal boundary layer or conduction layer. This should not be referred to as the lithosphere, which is a mechanical concept, but if the lithospheric thickness is thermally controlled, the thickness of the lithosphere should be proportional to the thickness of the thermal boundary layer.
5. The seismic LID. This is a region of high seismic velocity that overlies the low-velocity zone. At high temperatures the seismic moduli measured by seismic waves may be relaxed, in which case they can be of the order of 10 percent less than the high-frequency or unrelaxed moduli. High-temperature dislocation relaxation and partial melting are two mechanisms that serve to decrease seismic velocities. The boundary between the LID and the LVZ would be diffuse and frequency dependent if thermal relaxation is the mechanism. **A** sharp interface would be evidence for a chemical or mineralogical boundary.

There are several other pieces of data regarding the nature of the lithosphere. It has recently been found that the earthquakes in some subduction zones lie along two planes about 30 km apart. These may represent the top and bottom interfaces of the downgoing slab or internal interfaces in the slab or zones of maximum stress in the slab. The separation of the two seismic zones is similar to the flexural thickness of the plate.

The best evidence for cooling of the oceanic plate, or thickening of the thermal boundary layer, comes from the deepening of bathymetry as a function of time. The simple square-root of time relationship for bathymetry falls down after 80 million years, indicating that the thermal boundary layer has reached an equilibrium thickness or that a thermal

event prior to 80 Ma affected the parts of the oceanic lithosphere that have been used to calculate the bathymetry-age relation. The conductive cooling calculation apparently does not work in reverse: As the plate approaches a hotspot, it thins very rapidly to a thickness of about 30 km (Crough and Thompson, 1976). This thickness seems to be independent of plate rate or original plate thickness. Conductive heating is too slow to explain these results; mechanical thinning or delamination seems required in order to explain the heating time scale, and compositional or mineralogical control seems required in order to explain the equilibrium thickness obtained upon heating. The similarity in thickness of the heated lithosphere, the flexural lithosphere and the double seismic zone should be noted. These results suggest that there is a strong, refractory layer that extends to a depth of about 30 to 50 km. The material below this depth apparently is easily abraded, ablated or delaminated and is weaker than the subcrustal layer. This change in mechanical properties may be controlled by temperature, mineralogy, partial melting or stress.

EFFECTIVE ELASTIC THICKNESS OF THE LITHOSPHERE

We can now estimate the thickness of the "rheological lithosphere." Clearly it is a function of lithospheric age, the magnitude of the load, and the duration of loading. At a given depth, and therefore temperature, the rheology will appear elastic for times shorter than the characteristic relaxation time, and viscous for longer duration loads. The "thickness of the lithosphere" is therefore a more complicated concept than has been generally appreciated.

Figure 7-3 gives estimates of the thickness of the oceanic rheological lithosphere as a function of age of crust and duration of load, using oceanic geotherms and a stress of 1 kilobar. The depth to the rheological asthenosphere is defined as the depth having a characteristic time equal to the duration of the load. For example, from Figure 7-3 a 30-Ma-old load imposed on 80-Ma-old crust would yield a thickness of 45 km if the lithosphere did not subsequently cool, or if the cooling time is longer than the relaxation time. A 30-Ma-old load on currently 50-Ma-old crust would give a rheological lithosphere 34 km thick with the above qualifications. The thickness of the high seismic velocity layer overlying the low-velocity zone (the LID) is also shown in Figure 7-3. For load durations of millions of years, the rheological lithosphere is about one-half the thickness of the older estimates of the thickness of the seismological lithosphere. Note that the rheological thickness decreases only gradually for old loads. This is consistent with the observations of Watts and others (1975). On the other hand, the lithosphere appears very thick for young loads, and the apparent thickness decreases rapidly.

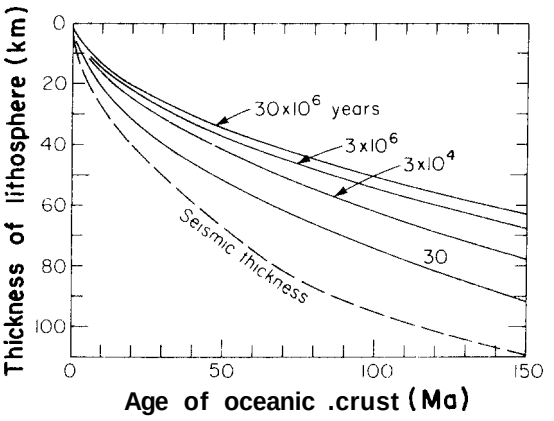

FIGURE **7-3**
Relationship between thickness of "elastic" lithosphere, age of oceanic crust and duration of loading for 1 kbar stress. For a given load the elastic thickness decreases with time. The dashed line is the upper bound of seismic determinations of LID thicknesses. Compare with Figure **3-2.**

MELTING AND ORIGIN OF MAGMAS

There are several ways to generate melts in the mantle. Melting can occur in situ if the temperature is increasing and eventually exceeds the solidus. The main source of heating in the mantle is the slow process of radioactive decay. Heating also leads to buoyancy and convection, a relatively rapid process that serves to bring heated material toward the surface where it cools. The rapid ascent of warm material leads to decompression, another mechanism for melting due to the relative slopes of the adiabat and the melting curve. Extensive in situ melting, without adiabatic ascent, is unlikely except in deep layers that are intrinsically denser than the overlying mantle. In this case melting can progress to a point where the intrinsic density contrast is overcome by the elimination of a dense phase such as garnet. Below about 100 km the effect of pressure on the melting point is much greater than the adiabatic gradient or the geothermal gradient in homogeneous regions of the mantle. Recent work on the melting of peridotites at high pressure shows that the melting curve levels off at pressures greater than about 100 kb. This combined with chemical boundary layers at depth makes it possible to envisage the onset of melting at depths between about 300 and 400 km or deeper. Because of the high temperature gradient at the interface between chemically distinct layers, melting is most likely to initiate in chemical boundary layers. Whether melting is most extensive above or below the interface depends on the mineralogy and the amount of the lower-melting-point phase. The Earth is slowly cooling with time and therefore melting was more extensive in the past and probably extended, on average, to both shallower and greater depths than at present.

Most experimental petrology is performed at pressures less than 40 kilobars, and it is natural that most theories of petrogenesis have been shoehorned into this accessible pressure range. The extrapolation of melting gradients obtained at low pressure suggest that plausible mantle temperatures are well below the solidus at depths greater than about 200 km.

Melting most likely is the result of adiabatic ascent from greater depth, initiating where the geotherm intersects the solidus. The amount of melting depends on the temperature interval between the solidus and the liquidus, the latent heat of fusion and the ability of the melt to leave the matrix.

Fragmentary evidence at high pressure (—100 kbar) indicates that the solidus and liquidus tend to converge at high pressure and that the effect of pressure on both decreases rapidly (Ohtani et al., 1986, Takahashi, 1986). Additionally, the MgO content of the initial melt increases with pressure, and the density of the melt and residual crystals converge with depth. These factors mean that high-MgO melts such as picrites and komatiites, or even peridotites, can be generated at depth, that extensive melting can occur upon further adiabatic ascent, and that melt separation is more likely at shallow depth than at great depth. The possible increase of melt viscosity with pressure and pinching off of permeability in a rapidly rising diapir will also affect melt separation at depth.

The dependence of melting point T_m on pressure is governed by the Clausius-Clapeyron equation

$$dT_m/dP = \Delta V/\Delta S = \text{TAVIL}$$

where AV and AS are the changes in volume and entropy due to melting and L is the latent heat of melting. AS is always positive, but AV can be either positive or negative. Therefore the slope of the melting curve can be either negative or positive but is generally positive. Although this equation is thermodynamically rigorous, it does not provide us with much physical insight and is not suitable for extrapolation since ΔV, AS and L all depend on pressure. Because of the high compressibility of liquids, A V decreases rapidly with pressure, and $\Delta V/V$ and AS probably approach limiting values at high pressure.

Lindemann proposed that melting occurs when the thermal oscillation of atoms reached a critical amplitude,

$$T_m = Am\theta^2V^{2/3}$$

where m is the mass of the atoms, V is the volume, θ is the Debye temperature and A is a constant. Gilvarry (1956) reformulated the equation in terms of the bulk modulus and volume of the solid at the melting point.

Other theories of melting propose that some critical density of dislocations or vacancies causes the crystal to melt or that a crystal becomes unstable when one of the shear moduli vanishes.

All of the above theories can be criticized because they do not involve the properties of the melt or considerations of solid-melt equilibrium. They correspond rather to an absolute stability limit of a crystal, which may differ from the crystal-liquid transition.

Stacey and Irvine (1977) were able to derive a melting relation, which resembles Lindemann's equation, from a simple adaptation of the Mie-Griineisen equation without involving the vibration amplitude assumption. An appropriate form of their equation *is*

$$dT_m/T_m\,dP = 2(\gamma - 2\gamma^2\alpha T_m)/K_T$$

The Lindemann law itself can be written

$$dT_m/T_m\,dP = 2(\gamma - 1/3)/K_T$$

which gives almost identical numerical values. These can be compared with the expression for the adiabatic gradient

$$dT/T\,dP = \gamma/K_T$$

Since γ is generally about 1, the melting point gradient is steeper *than the adiabatic gradient.* Far $\gamma < 213$ the reverse is true.

If the above relations apply to the mantle, the adiabat and the melting curve diverge with depth. This means that melting is a shallow-mantle phenomenon and that deep melting will only occur in thermal boundary layers in a convecting mantle. In thermal boundary layers the thermal gradient is controlled by the conduction gradient, which is typically 10–20°C/km compared to the adiabatic gradient of 0.3°C/km. A limited amount of data at very high pressure indicates that dT_m/dP decreases with pressure, and T_m may approach a constant value. The adiabatic gradient, of course, also decreases with pressure.

The Lindemann law was motivated by the observation that the product of the coefficient of thermal expansion a and the melting temperature T_m was very nearly a constant for a variety of materials. This implies that

$$dT_m/dP = -(T_m/\alpha)(\partial\alpha/\partial P)_T$$

which can be written

$$dT_m/T_m\,dP = -(\partial \ln K_T/\partial \ln V)_P/K_T$$
$$= -(1/\alpha K_T^2)(\partial K_T/\partial T)_P$$

Thus, the increase of melting temperature with pressure can be estimated from the thermal and elastic properties of the solid. Typical values for silicates are T_m, ~2000K, $-(\partial \ln K_T/\partial \ln V)_P$ —5 and K_T, —1500 kbar, giving

$$dT_m/dP \approx 6°C/\text{kbar}$$

which is in the ballpark of observed values. For example, the mean slopes of the melting curves for albite, enstatite, diopside and pyrope at pressures below 10–30 kb range from 5 to 15°C/kbar (see Table 7-5). Metals generally have an initial melting point gradient of 3 to 9 K/kilobar.

The Simon fusion equation,

$$P_m/P_o = (T_m/T_o)^c - 1$$

TABLE 7-5
Calculated and Measured Initial Melting Point Gradients

Mineral	Calculated dT_m/dP	Measured dT_m/dP
Mg_2SiO_4	9.7	4.8
$MgSiO_3$	11.2	12.8
Diopside	9.7	13 (5 kbar)
		7.5 (50 kbar)

$(T_m)^{-1}\ dT_m/dP\ (calculated) = -(\partial \ln K_S/\partial\ In\ V)_P/K_S$

has received much attention in the geophysics literature. T_o is the melting temperature at zero pressure and P_o and c are constants. Gilvarry (1956) showed the equivalence of this to the Lindemann equation by invoking the "law of corresponding states"

$$T_m/T_o = (V_o/V_m)^{2(\gamma - 1/3)}$$

and obtained

$$c = (6\gamma + 1)/(6\gamma - 2)$$

P_o is the (negative) melting pressure at zero temperature.

Although silicates are complex multicomponent systems, the solidi of many natural systems typically have slopes of 10–15°C/km. The presence of volatiles such as water and CO_2 considerably reduces the initial melting point, or solidus, of silicates at low pressure, but the behavior at higher pressure and the behavior of the liquidus are relatively simple.

Stacey (1977), attempting to estimate the melting temperature in the mantle from seismic data using considerations similar to the above, obtained a T_m of 3157 K at the base of the mantle as shown in Table 7-6. Ohtani (1983) used measured and estimated melting information on various silicates and extrapolated these, also using solid-state physics considerations. His results for the liquidus and solidus temperature profiles are also given in the table. Stacey's

TABLE 7-6
Estimates of Temperature (T), Melting Temperature (T_m), Liquidus Temperature (T_l), Solidus Temperature (T_s) and Debye Temperature (θ) for the Mantle (All in K)

Depth (km)	T	T_m	T_l	T_s	θ	γ
600	2230	2300	2800	2300	900	0.74
1100	2400	2500	3500	3000	1100	1.00
1500	2600	2700	4200	3800	1200	0.97
1900	2700	2800	5500	4500	1250	0.95
2200	2800	2950	6000	4900	1300	0.94
2900	3200	3200	6500	5000	1400	0.91

Stacey *(1977);T and* T_s from *Ohtani (1983).*

TABLE 7-7
Selected Ionic Radii (Å)

Ion	Coordination	Radius
Al^{3+}	IV	0.39
	V	0.48
	VI	0.535
As^{3+}	VI	0.58
As^{5+}	IV	0.335
	VI	0.46
B^{3+}	III	0.01
	IV	0.11
	VI	0.27
Ba^{2+}	VI	1.35
	VII	1.38
	VIII	1.42
	IX	1.47
Ba^{2+}	X	1.52
	XI	1.57
	XII	1.61
Be^{2+}	IV	0.27
	VI	0.45
Br^-	VI	1.96
C^{4+}	III	−0.08
	IV	0.15
Ca^{2+}	VI	1.00
	VII	1.06
	VIII	1.12
	IX	1.18
	X	1.23
Ca^{2+}	XII	1.34
Cd^{2+}	VI	0.95
Ce^{4+}	VIII	0.97
Cl^-	VI	1.81
Co^{2+}(HS)*	VI	0.745
Cr^{2+}(HS)	VI	0.80
Cr^{3+}	VI	0.615
Cs	VI	1.67
	VIII	1.74
	XI	1.88
Eu^{+2}	VI	1.17
	VIII	1.25
F^-	IV	1.31
	VI	1.33
Fe^{2+}(HS)	IV	0.63
	IV	0.64
(HS)	VI	0.780
	VIII	0.92
Fe^{3+}	IV	0.49
(HS)	VI	0.645
Ga^{3+}	IV	0.47
Ge^{4+}	IV	0.39
	VI	0.53
H^+	I	−0.38
	II	−0.18
Hf^{4+}	VI	0.71
	VIII	0.83
Hg^{2+}	VI	1.02
I^-	VI	2.20
K^+	VI	1.38

TABLE 7-7 (continued)
Selected Ionic Radii

Ion	Coordination	Radius
	VIII	1.51
	IX	1.55
	X	1.59
	XII	1.64
Li^{+}	IV	0.59
	VI	0.76
	VIII	0.92
Mg^{2+}	IV	0.57
	VI	0.720
	VIII	0.89
Mn^{2+}(HS)	VI	0.830
	VIII	0.96
Mn^{3+}(HS)	VI	0.645
N^{3-}	IV	1.46
N^{3+}	VI	0.16
N^{5+}	III	−0.10
Na	VI	1.02
	VII	1.12
	VIII	1.18
	IX	1.24
	XII	1.39
Ni^{2+}	IV	0.55
	VI	0.690
O^{2-}	II	1.35
	III	1.36
	IV	1.38
	VI	1.40
	VIII	1.42
OH^{-}	II	1.32
	III	1.34
	IV	1.35
	VI	1.37
P^{5+}	IV	0.17
	VI	0.38
Pb^{2+}	VI	1.19
	VIII	1.29
Rb^{+}	VI	1.52
	VIII	1.61
	IX	1.63
	X	1.66
	XII	1.72
Ru^{4+}	VI	0.62
S^{2-}	VI	1.84
Se^{2-}	VI	1.98
Si^{4+}	IV	0.26
	VI	0.40
Sm^{3+}	VI	0.96
Sn^{4+}	VI	0.69
Sr^{2+}	VI	1.18
	VIII	1.26
	XII	1.44
Te^{2-}	VI	2.21
Ti^{3+}	VI	0.670
Ti^{4+}	IV	0.42
	VI	0.605
U^{4+}	VI	0.89
	VIII	1.00
V^{2+}	VI	0.79
V^{3+}	VI	0.64
V^{5+}	IV	0.355
	VI	0.54
W^{4+}	VI	0.66
Zn^{2+}	IV	0.60
	VI	0.74
Zr^{4+}	VI	0.72
	VIII	0.84

Shannon (1976).
* (HS) denotes high-spin electronic configuration.

estimated geotherm is given for comparison. The T_m calculation of Stacey is much lower than T_1 of Ohtani, partly because he assumed that both the top and base of the mantle are at the melting point, not just locally but on average. Ohtani's estimated melting temperatures diverge rapidly from the geotherm with increasing depth in the lower mantle.

Also given in Table 7-6 are Stacey's estimates of the Debye temperature, θ, and the Grüneisen ratio, y, both estimated from the seismic data. For comparison, the estimated variations of heat capacity C_P throughout the mantle is only about 1 percent, and the coefficient of thermal expansion, α, decreases by about a factor of 2 or 3.

IONIC RADII

Crystal chemists and other investigators have found the concept of ionic radii to be extremely useful. Atoms and ions are treated as hard spheres, and empirical tables of atomic and ionic radii have been computed that closely reproduce interatomic distances. Approximate additivity of atomic and ionic radii was noted by the earliest investigators. The principle of additivity of cation and anion radii in ionic crystals accurately reproduces interatomic distances if one takes into consideration the coordination number, electronic spin, covalency and repulsive forces. Ionic radii have been important to crystal chemists because structure types and coordinations are determined by cation/anion radius ratios. For example, the likely crystal structures of high-pressure phases can often be inferred from these ratios. The geochemist uses these radii to infer what ions can readily substitute for others. Thus, partition coefficients depend on ionic radii. Elasticity systematics also depend on ionic radii. Diffusivity, anelasticity and activation volumes depend on the size of the diffusing species. Table 7-7 gives ionic radii as determined by Shannon and Prewitt (1969) and Shannon

TABLE 7-8
Measured Variation of K_s with Temperature and Pressure and Intrinsic Temperature Dependence

Mineral	α (10^{-6}/K)	$(\partial \ln K_S/\partial \ln V)_T$	$(\partial \ln K_S/\partial \ln V)_P$	$\alpha^{-1}(\partial \ln K_S/\partial T)_V$
Al_2O_3	16.4	−4.3	−4.1	+0.2
Mg_2SiO_4	24.7	−4.8	−5.7	−0.9
Olivine	24.7	−5.4	−4.7	+0.7
Pyroxene	47.7	−9.5	−5.5	+4.0
$MgAl_2O_4$	22.0	−4.9	−3.7	+1.2
Quartz	36.6	−6.4	−5.8	+0.6
Garnet	21.6	−5.5	−5.2	+0.3
Garnet	19.0	−4.8	−5.9	−1.1
MgO	31.5	−3.8	−3.1	+0.7
$SrTiO_3$	28.2	−5.7	−7.7	−2.0

$$\underset{\text{(measured)}}{\left(\frac{\partial \ln K}{\partial \ln V}\right)_P} = \underset{\text{(measured)}}{\left(\frac{\partial \ln K}{\partial \ln V}\right)_T} + \alpha^{-1}\underset{\text{(computed)}}{\left(\frac{\partial \ln K}{\partial T}\right)_V}$$

(1976). The variation of the adiabatic bulk modulus with volume is given in Table 7-8 for some important crystals.

General References

Ashby, M. F. and R. A. Verrall (1978) Micromechanism of flow and fracture, and their relevance to the rheology of the upper mantle, ***Phil. Trans. R. Soc. Lond. A., 288,*** 59–95.

Hirth, J. P. and J. Lothe (1968) ***Theory of Dislocations,*** McGraw-Hill, New York, 780 pp.

Jaoul, O., M. Poumellec, C. Froidevaus and A. Havette (1981) Silicon diffusion in forsterite: A new constraint for understanding mantle deformation. In ***Anelasticity in the Earth*** (F. D. Stacey, M. S. Patterson, A. Nicholas, eds.), 95–100, American Geophysical Union, Washington, D.C.

Nicolas, A. and J. P. Poirer (1976) ***Crystalline Plasticity and Solid State Flow in Metamorphic Rocks,*** John Wiley and Sons, London, 444 pp.

Nowick, A. S. and B. S. Berry (1972) ***Anelastic Relaxation in Crystalline Solids,*** Academic Press, New York, 677 pp.

Stacey, F. (1977) Applications of thermodynamics to fundamental Earth physics, ***Geophys. Surveys, 3,*** 175–204.

References

Anderson, D. L. (1967) The anelasticity of the mantle, ***Geophys. J. Roy. Astron. Soc., 14,*** 135–164.

Berckhemer, H., F. Auer and J. Drisler (1979) High-temperature anelasticity and elasticity of mantle peridotite, ***Phys. Earth Planet. Inter., 20,*** 48–59.

Borelius, G. (1960) ***Arkiv Fysik, 16,*** 437.

Creager, K. and T. Jordan (1984) Slab penetration into the lower mantle, ***J. Geophys. Res., 89,*** 3031–3050.

Crough, S. T. (1977) Isostatic rebound and power-law flow in the asthenosphere, ***Geophys. J. Roy. Astron. Soc., 50,*** 723–738.

Crough, S. T. (1979) Geoid anomalies across fracture zones and the thickness of the lithosphere, ***Earth Planet. Sci. Lett., 44,*** 224–230.

Crough, S. T. and G. Thompson (1976) Numerical and approximate solutions for lithospheric thickening and thinning, ***Earth Planet. Sci. Lett., 31,*** 397–402.

Debye, P. (1912) ***Ann. Phys. Lpz., 39,*** 784.

Freer, ***R.*** (1981) Diffusion in silicate minerals and glasses, ***Contrib. Mineral. Petrol., 76,*** 440–454.

Fujisawa, H., N. Fujii, H. Mizutani, H. Kanamori and S. Akimoto (1968) Thermal diffusivity of Mg_2SiO_4, Fe_2SiO_4, and NaCl at high pressure and temperature, ***J. Geophys. Res., 73,*** 4727–4733.

Gilvarry, J. J. (1956) ***Phys. Rev.,*** 102, 317.

Gittus, J. (1976) ***Phil. Mag., 34,*** 401–411.

Goetze, C. and D. L. Kohlstedt (1973) Laboratory study of dislocation climb and diffusion in olivine, ***J. Geophys. Res., 78,*** 5961–5971.

Horai, K. (1971) Thermal conductivity of rock-forming minerals, ***J. Geophys. Res., 76,*** 1278–1308.

Horai, K. and G. Simmons (1970) An empirical relationship between thermal conductivity and Debye temperature for silicates, ***J. Geophys. Res., 75,*** 678–982.

Keyes, R. (1963) Continuum models of the effect of pressure on activated processes. In ***Solid Under Pressure*** (W. Paul and D. M. Warschauer, eds.), 71–99, McGraw-Hill, New York.

Kobayzshigy, A. (1974) Anisotropy of thermal diffusivity in olivine, pyroxene and dunite, ***J. Phys. Earth, 22,*** 359–373.

Kohlstedt, D. L. and C. Goetze (1974) Low-stress high-temperature creep in olivine single crystals, *J. Geophys. Res., 79,* 2045–2051.

Minster, J. B. and D. L. Anderson (1980) Dislocations and nonelastic processes in the mantle, *J. Geophys. Res., 85,* 6347–6352.

Minster, J. B. and D. L. Anderson (1981) A model of dislocation-controlled rheology for the mantle, *Phils. Trans. R. Soc. London A, 299,* 319–356.

Ohtani, E. (1983) Melting temperature distribution and fractionation in the lower mantle, *Phys. Earth Planet. Inter., 33,* 12–25.

Ohtani, E., T. Kato and H. Sawamoto (1986) *Nature, 322,* 352–353.

Sammis, C., J. Smith, G. Schubert and D. Yuen (1977) Viscosity-depth profile of the Earth's mantle; effects of polymorphic phase transitions, *J. Geophys. Res., 82,* 3747–3761.

Schatz, J. F. and G. Simmons (1972) Thermal conductivities of Earth materials at high temperatures, *J. Geophys. Res., 77,* 6966–6983.

Shannon, R. D. (1976) *Acta Cryst., A32,* 751.

Shannon, R. D. and C. T. Prewitt (1969) *Acta Cryst.,* 925.

Stacey, F. D. (1977) A thermal model of the Earth, *Phys. Earth Planet. Inter., 15,* 341–348.

Stacey, F. D. and R. D. Irvine (1977) *Austral. J. Phys., 30,* 631.

Takahashi, E. (1986) *J. Geophys. Res., 91,* 9367–9382.

Watts, A. B., J. R. Cochran and G. Selzer (1975), Gravity anomalies and flexures of the lithosphere: A three-dimensional study of the Great Meteor Seamount, N. E. Atlantic, *J. Geophys. Res., 80,* 1391–1398.